Global Change Biology

Supporting Information

Soil enzymes as indicators of soil function: a step toward greater realism in microbial ecological modeling

Gangsheng Wang[1,2*], Qun Gao[3], Yunfeng Yang[3], Sarah E Hobbie[4], Peter B Reich[5,6] and Jizhong Zhou[2,7,8*]

[1]Institute for Water-Carbon Cycles and Carbon Neutrality, and State Key Laboratory of Water Resources and Hydropower Engineering Sciences, Wuhan University, Wuhan 430072 China

[2]Institute for Environmental Genomics, and Department of Microbiology and Plant Biology, University of Oklahoma, Norman, OK 73019, USA

[3]State Key Joint Laboratory of Environment Simulation and Pollution Control, School of Environment, Tsinghua University, Beijing 100084, China

[4]Department of Ecology, Evolution, and Behavior, University of Minnesota, St Paul, MN 55108 USA

[5]Department of Forest Resources, University of Minnesota, St Paul, MN 55108 USA

[6]Hawkesbury Institute for the Environment, Western Sydney University, Penrith, New South Wales 2753, Australia.

[7]School of Civil Engineering and Environmental Sciences, University of Oklahoma, Norman, OK 73019, USA

[8]Earth and Environmental Sciences, Lawrence Berkeley National Laboratory, Berkeley, CA 94720, USA

[*]Corresponding authors. E-mail: wang.gangsheng@gmail.com and jzhou@ou.edu

1. Microbial-ENzyme Decomposition (MEND) Model

1.1.MEND model description

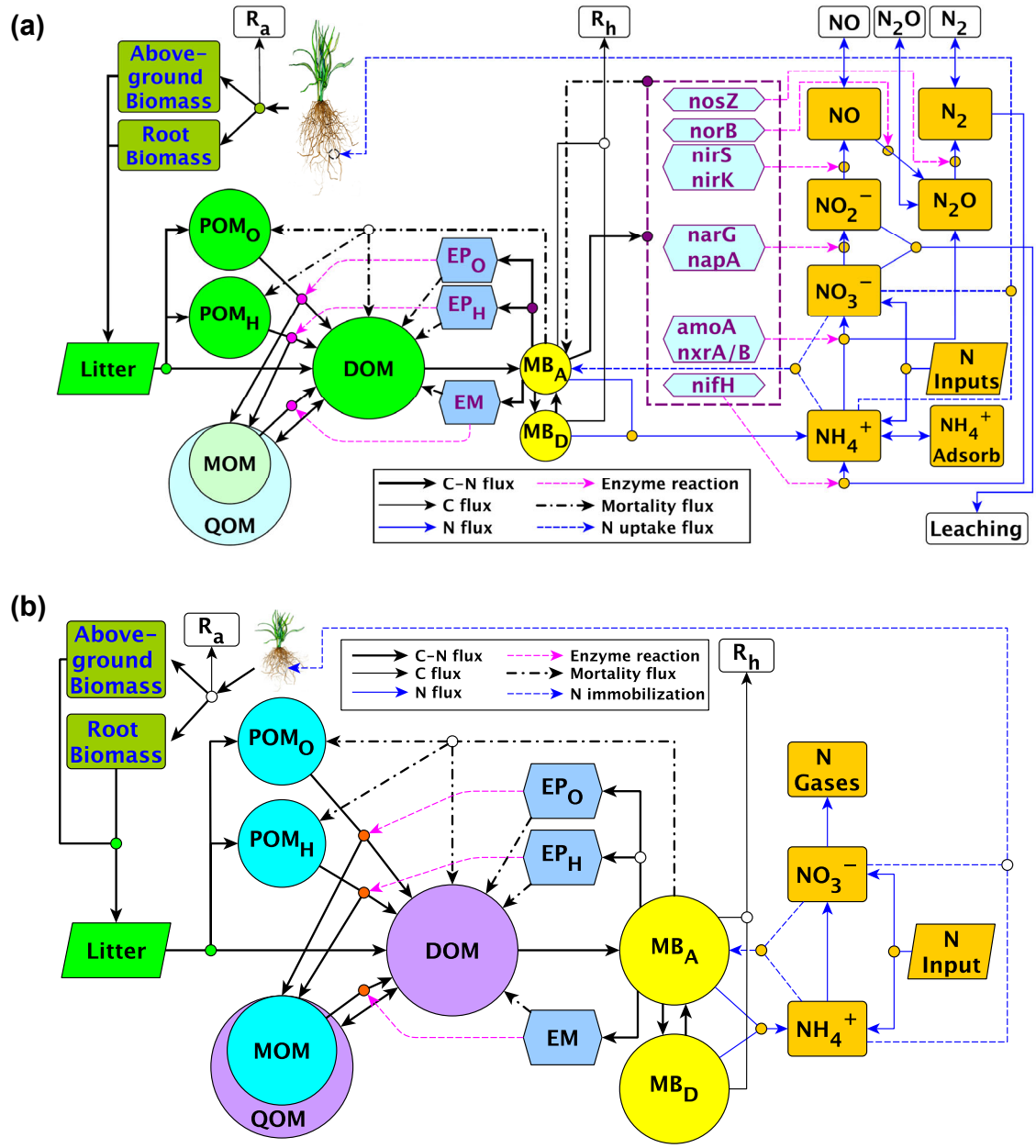

Figure S1 Diagram of the MEND model. **(a)** New version of MEND model developed in this study; **(b)** Old version of MEND with simplified N processes as described in Gao et al. [1] and Wang et al. [2].

The MEND model (Fig. S1a) [3-5] allows for mechanistic representation of (i) density-based partitioning and physicochemical protection of soil organic matter (SOM) (Fig. S1b); (ii) distinct microbial and enzyme groups regulating SOM decomposition and inorganic nitrogen (N) transformations including N mineralization & immobilization, biological N fixation, nitrification, and sequential denitrification; (iii) microbial physiology such as growth & maintenance, dormancy & resuscitation, and mortality in response to changes in soil pH, temperature, and moisture; (iv) plant-microbial competition for inorganic N (NH_4^+ and NO_3^-); (v) ammonium (NH_4^+) sorption and nitrate (NO_3^-) & nitrite (NO_2^-) leaching; and (vi) N gases (NO, N_2O, and N_2) exchange between soil and the atmosphere (Fig. S1a). Model state variables, governing equations, component fluxes and parameters are described in Supplementary Table S1–S5.

1.1.1. Soil carbon (C) and nitrogen (N) pools

The MEND model includes the following soil C-N pools (Table S1):

Five SOM (with both C & N) pools: particulate organic matter (POM) decomposed by oxidative enzymes (POM_O), POM decomposed by hydrolytic enzymes (POM_H), mineral-associated organic matter (MOM), dissolved organic matter (DOM), and active MOM (QOM) interacting with DOM via sorption and desorption.

Seven inorganic N pools: adsorbed ammonium (NH_4^+ Adsorb), non-adsorbed ammonium (NH_4^+), nitrate (NO_3^-), nitrite (NO_2^-), nitric oxide (NO), nitrous oxide (N_2O), and dinitrogen (N_2).

Two microbial (with both C & N) functional groups: active and dormant microbes (MB_A and MB_D).

Three enzyme functional groups for SOM decomposition: POM_O-degrading enzymes (EP_O), POM_H-degrading enzymes (EP_H), and MOM-degrading enzymes (EM).

Six enzymes as bioindicators controlling inorganic N transformations: nitrogenases (corresponding to functional genes of nifH), ammonia oxidases (amoA & nxrA/B), nitrate reductases (narG/napA), nitrite reductases (nirS/nirK), nitric oxide reductases (norB), and nitrous oxide reductases (nosZ) [6, 7].

The governing (C or N mass balance) equations for these C-N pools are summarized in Table S2, where Eq. 13 shows the overall soil C mass balance and Eqs. 23a–c indicate the mass balance of soil organic N, inorganic N, and total N, respectively.

1.1.2. Flexible stoichiometry

In contrast to traditional models that use fixed SOM C:N ratios [8, 9], we use flexible stoichiometry (i.e., time-variant C:N ratio) for SOM and microbial biomass pools to represent the adaption of microbes in response to the stoichiometric imbalance of available resources [10-14]. One exception is for the enzyme pools, where a fixed C:N ratio (=3) is used according to Schimel and Weinstraub [15]. Generally, the organic N flux will follow the organic C flux according to the C:N ratio in the upstream (source) pool (see Eq. 14 in Table S2). The C:N ratios in the SOM pools (including POM_O, POM_H, MOM, QOM, DOM) will be regulated by the litter input, C-N flux from upstream pool, and/or microbial turnover. The C:N ratio in the microbial biomass pool is self-regulated by the DOM uptake, heterotrophic respiration (R_h), N mineralization and immobilization. R_h is mainly controlled by the intrinsic C use efficiency (Y_g or intrinsic CUE) (see Eqs. 33–37 in Table S3). In addition to the availability of DON and inorganic N (NH_4^+ and NO_3^-), we define an intrinsic N use efficiency (YN_g or intrinsic NUE, see Eq. 47 in Table S4) to modify N mineralization rate (Eq. 46 in Table S4) and immobilization rates (Eqs. 48–49). In Eq. 47, we first assume a conservative C:N range (i.e., between $CN_{BA,min}$ and $CN_{BA,max}$) to represent the stoichiometric plasticity of microbial communities [10, 14, 16]. Intrinsic NUE (YN_g in Eq. 47) will

increase with increasing microbial C:N ratio (CN_{BA}), with YN_g being 0 when $CN_{BA} \leq CN_{BA,min}$ (C-limited) and YN_g approaching 1 when $CN_{BA} \geq CN_{BA,max}$ (N-limited). This means that N mineralization rate will decrease, and N immobilization rate will increase when microorganisms become more N limited, resulting in higher YN_g [13].

1.1.3. SOM decomposition

The decomposition of POM_O, POM_H, and MOM pools is modeled by the Michaelis-Menten kinetics [17, 18]. The decomposition flux is determined by the concentration of a SOM pool and its corresponding enzymes (e.g., POM_O and EPo), as well as two kinetic parameters, i.e., the specific enzyme activity and the half-saturation constant (Vd and K) (see Eqs. 24–26 in Table S3).

1.1.4. DOM sorption and desorption

The sorption and desorption between DOM and QOM are simultaneously considered as dynamic processes [5]. DOM adsorption is controlled by DOM concentration and mineral surface coverage, and desorption is presumed to only depend on surface coverage (Eqs. 27–28 in Table S3). Relative saturation of the QOM pool (i.e., Q/Q_{max}, ratio of actual adsorbed C content to the sorption capacity) is defined to represent the fraction of the mineral surface area occupied [5].

1.1.5. Microbial growth, maintenance, and mortality

Microbial growth and maintenance are described by the Compromise model that combines the features of the Pirt model and the Herbert model [19]. The Compromise model explicitly expresses the dependence of microbial maintenance on both microbial biomass and substrate (DOM) availability (Eqs. 29, 33–34 in Table S3). We define a parameter ($\alpha = V_m /(V_g + V_m) \leq 0.5$) to constrain the relationship between the maximum specific growth and maintenance rate (V_g and V_m) (Eq. 29). The maintenance rate of dormant microbes is much lower than that of active microbes

by a factor of β = 0.001–0.01 (Eq. 36) [3]. Microbial mortality rate ($\gamma \cdot V_m$ in Eq. 32) is associated with the maintenance rate by a scaling factor (γ).

1.1.6. Microbial dormancy and resuscitation

When environmental conditions are unfavorable for growth, microbes may enter a state of low metabolic activity (i.e., dormancy) until conditions improve to allow replication [20, 21]. We simulate microbial dormancy and resuscitation as reversible dynamic processes (Eqs. 30–31 in Table S3), which are mainly determined by the availability of DOM and soil moisture.

1.1.7. Competitive dynamic enzyme allocation and turnover

We propose a competitive dynamic enzyme allocation scheme to deal with the synthesis of multiple enzymes (e.g., eight groups in this study). The enzyme allocation approach developed here is based on the synthetic results that enzyme activities are dependent on microbial biomass [22] and substrate availability [23]. The synthesis of SOM-degrading enzymes (EP_O, EP_H and EM) depends upon the active microbial biomass and the relative abundance of the C substrate that needs to be decomposed (Eq. 38) [3]. Given that the synthesis of SOM-degrading enzymes has been calculated in advance, the total synthesis rate of all inorganic-N enzymes is assumed to be proportional to the total synthesis rate of all SOM-degrading enzymes by a scaling factor, which is defined as the ratio of total soil inorganic N to total soil organic N ($(NH4 + NO3 + NO2)/\sum_{i=1}^{4} SON_i$) (Eq. 40). A competitive allocation scheme is applied to the production of enzymes for each inorganic-N transformation process, where the competitive allocation coefficient is the saturation level of an inorganic N substrate (i.e., N_j/KSN_j, the ratio of the substrate concentration to the half-saturation constant) compared to the overall saturation level of all inorganic N substrates ($\sum_{j=1}^{6}\left(N_j/KSN_j\right)$) (Eq. 40). Enzyme turnover is proportional to the enzyme concentration by the turnover rate (Eqs. 39 and 41). The turnover of extracellular enzymes (EP_O, EP_H and EM) enters

the DOM pool, whereas the turnover of intracellular enzymes (nitrogenase, ammonia oxidases, and N-reductases) becomes microbial biomass, as these N-enzymes are located at cell membrane, cytoplasm, or periplasm [24-26].

1.1.8. Soil respiration

MEND simulates soil respiration (R_s) as the sum of autotrophic (root) respiration (R_a) and heterotrophic (microbial) respiration (R_h), where R_a is calculated as a fraction ($f_{Ra} \in (0.1,0.4)$) of gross primary production (GPP, g C m^{-2} d^{-1}); and R_h is the sum of microbial growth respiration ($R_{h,g}$), maintenance respiration ($R_{h,g}$), and overflow respiration ($R_{h,g}$) (see Eqs. 10–12 in Table S2 and Eqs. 33–37 in Table S3. Microbes may release CO_2 via overflow respiration to make the microbes meet their stoichiometry constraint (i.e., maximum allowed microbial C:N ratio) [27, 28].

1.1.9. Microbial N mineralization and plant-microbial competition for inorganic N

Based on our definition of intrinsic NUE (YN_g in Eq. 47), a fraction (YN_g) of ingested DON is incorporated into microbial biomass and the rest is mineralized (Eq. 46). We adapted the Equilibrium Chemistry Approximation (ECA) kinetics [29] to model the plant-microbial competition for inorganic N (NH_4^+ and NO_3^-) (Eqs. 48–52).

1.1.10. Biological N fixation, nitrification, and denitrification

The biological N fixation (BNF), nitrification, and denitrification processes are simulated via the Michaelis-Menten kinetics, with each reaction being mediated by the corresponding enzyme groups. The BNF rate is also modified by the soil NH_4^+ availability (quantified by the saturation level of NH_4^+), i.e., higher soil NH_4^+ availability will inhibit N fixation (Eq. 45) [30]. The nitrification and denitrification chain reactions ($NO_3^- \rightarrow NO_2^- \rightarrow NO \rightarrow N_2O \rightarrow N_2$) are catalyzed by specific enzymes (Eqs. 42 and 44). In addition, nitrifier-denitrification flux is modeled as a

fraction of the nitrification flux and contributes to N_2O production [31, 32], where the fraction is controlled by oxygen availability (Eq. 43).

1.1.11. Ammonium (NH_4^+) sorption and nitrate (NO_3^-) & nitrite (NO_2^-) leaching

We also consider the sorption of NH_4^+ using the Langmuir isotherm model (Eq. 53) [33]. Only the un-adsorbed NH_4^+ is available for microbial and plant uptake. The leaching of NO_3^- and NO_2^- is controlled by the concentration of NO_3^- and NO_2^- in soil solution as well as the amount of soil water percolation (Eq. 54) [34].

1.1.12. N gases (NO, N_2O, and N_2) exchange between soil and the atmosphere

N gases exchange between soil and the atmosphere is simulated by a diffusion process governed by the Fick's law (Eq. 55), i.e., the flux is mainly determined by the difference in gas concentrations between soil and the atmosphere as well as the gas diffusivity in soil. Gas diffusivity is dynamically calculated by internal and external air-filled porosities in bimodal (aggregated) soil porous media [35-37].

1.2. Soil pH, temperature and moisture response functions

Soil pH, temperature and moisture response functions are summarized in Table S6. A model parameter (e.g., reaction rate) in MEND may be modified by environmental conditions, such as soil water, temperature, and pH (Eq. 56 in Table S6):

The pH response function, $f(pH)$, follows an exponential-quadratic function (Fig. S2, Eq. 57 in Table S6) [38].

The temperature sensitivity of true growth yield or intrinsic carbon use efficiency (Y_g) is modeled by a linear function (Eq. 58 in Table S6) [39-44].

The Arrhenius equation (Eq. 59) or Q_{10} method (Eq. 60) is used to simulate the response of other parameters [5] to changes in temperature (Fig. S3). The relationship between Q_{10} and Ea (Eq.

61) is derived from Eqs. 59 and 60. The activation energy (*Ea*) for selected parameters is described in Wang et al., [5].

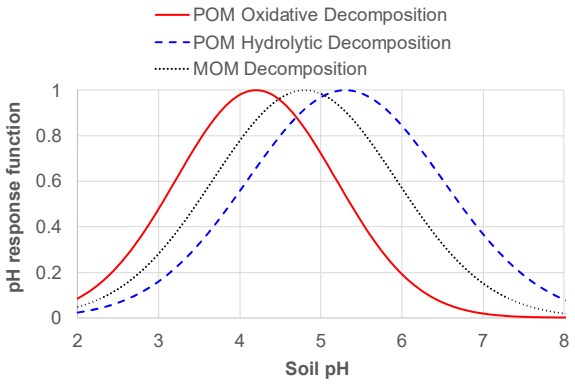

Figure S2 Soil pH response functions. POM and MOM are particulate and mineral-associated organic matter, respectively.

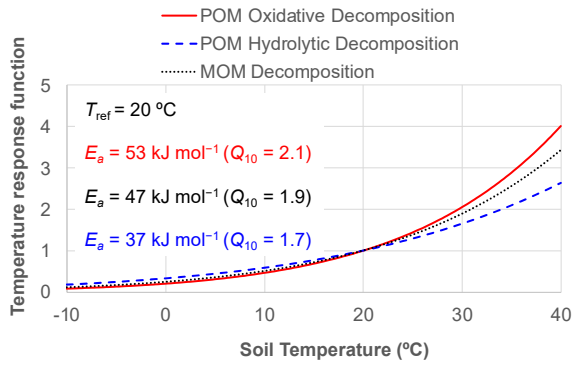

Figure S3 Soil temperature response functions. POM and MOM are particulate and mineral-associated organic matter, respectively; T_{ref} denotes the reference temperature in the response function; E_a is the activation energy when the Arrhenius Equation is used; and Q_{10} is the corresponding Q_{10} value.

We use different soil moisture response functions (SMRFs) [4] to describe the influences of soil moisture on the enzyme-mediated SOM decomposition processes, microbial mortality, microbial dormancy and resuscitation, nitrification and denitrification (Fig. S4).

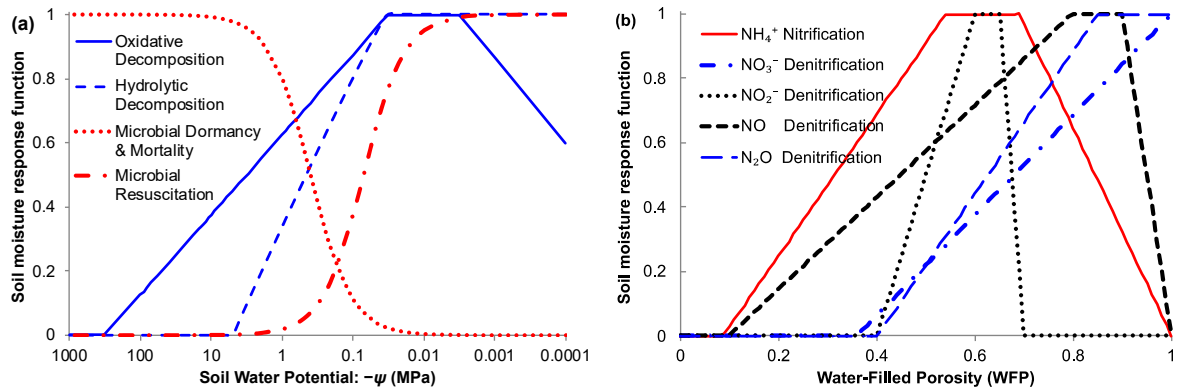

Figure S4 Soil moisture response functions for (a) oxidative and hydrolytic decomposition, microbial dormancy & mortality and resuscitation; (b) nitrification and denitrification.

(1) The SMRF for SOM decomposition by oxidative enzymes (Eq. 62 in Table S6) is adapted from Hansen et al. [45]. (Fig. S4a)

(2) The SMRF for SOM decomposition by hydrolytic enzymes (Eq. 63 in Table S6) is based on Manzoni et al. [46] (Fig. S4a). The values of ψ_{min} and b in Eq. 63 for soil or litter in different biomes were adapted from Manzoni *et al*. [46].

(3) The SMRFs for microbial mortality, dormancy & resuscitation are also shown (Eqs. 64 and 65 in Table S6) in Fig. S4a. Soil water potential greatly affects the microbial dormancy and reactivation processes and various sigmoidal-type switching functions have been proposed to quantify these effects [4, 47]. The response functions (Eqs. 64 and 65 in Table S6) are used to modify the dormancy ($f_{A2D}(\psi)$) and the reactivation ($f_{D2A}(\psi)$), where ψ is the SWP (MPa) and the exponent ω describes the steepness of the curve; ψ_{A2D} and ψ_{D2A} are critical SWPs depending on the osmolyte synthesis strategy; and τ is the ratio between ϕ_{D2A} and ϕ_{A2D} and is less than 1 to capture a lagged switch from dormant to active state upon rewetting [47]. We also use $f_{A2D}(\psi)$ to modify microbial mortality rate.

(4) The SMRFs for nitrification and denitrification (Eq. 66 in Table S6) are shown in Fig. S4b. The values for WFP_i, $(i = 1,2,3,4)$ and a_+, b_+, a_-, b_- are adapted from Muller [48] and Wang & Chen [37].

2. Model Initialization and Input Data

2.1. Model initialization

We initialize the C-N pool sizes (Table S1), at least for those SOM pools, by experimentally measured values. When data are not available, initial microbial and enzyme pool sizes may be estimated based on literature research. For example, MBC is usually 1–5% of SOC and may be further specified according to the biomes [49] or soil taxonomy [5]; enzyme concentrations are around 0.1–1% of MBC [3, 38].

If the modeling study is not focused on a well-controlled experiment with specific initial conditions and measurements, for example, a theoretic analysis or scenario analysis of the soil C-N cycle in response to environmental change, we may conduct a long-term (from 50 years to hundreds of years) model spin-up to reach a (dynamic) steady state [8, 50], which is used as initial conditions to continue model simulations under projected changes in environmental conditions.

2.2. Model input data

Model input data are used to drive model simulations and generally include: (i) litter input or GPP; (ii) soil pH, temperature and moisture; (iii) inorganic N (NH_4^+ and NO_3^-) input (e.g., dry/wet deposition and fertilization). Depending on the data availability, these input data may be provided as constant values or time-variant values at hourly, daily, monthly scale. All input data will be automatically interpolated or converted to hourly data for MEND model simulations. Soil texture and/or soil water retention curve parameters for the van Genuchten model [51, 52] are also needed

for modeling, where the soil water retention curve is used to convert volumetric water contents to soil water potentials [4, 53].

2.3. BioCON data

Soil CO_2 flux (soil respiration) in each plot was measured from 11 to 36 times per year using a LI-COR 6400-09 soil respiration chamber (LI-COR, Lincoln, Nebraska, USA). There were 284 time points of soil respiration fluxes for each treatment from 1998 to 2009. Plant C/N ratio (aboveground plant and root) and soil inorganic N pools and fluxes were measured in July–August of each year [1]. Soil NH_4^+ and NO_3^- in four removed soil cores were extracted with 1 M KCl and their concentrations were measured on an Alpkem autoanalyzer (OI Analytical, College Station, Texas, USA). Net N mineralization rates were calculated as the difference between the total inorganic N (NH_4^+ and NO_3^-) in the field-incubated PVC tubes and that in the soil cores removed roughly one month earlier. Net nitrification rates were estimated using only NO_3^- data [54].

3. Model Parameterization, Calibration and Validation

3.1. Model parameterization procedure

A rigorous model parameterization procedure is essential to avoid methodological problems in the subsequent model calibration and validation. We adopt the following procedure for model parameterization [55, 56]: (i) The parameter classes are determined based on site properties such as soil texture or types, plant functional types, and climatic zones, so that the parameter values in different classes could be assessable from available field data. (ii) The number of practically calibrated parameters should be kept as low as possible. This means to calibrate the most important and sensitive parameters and the other parameters should be fixed based on previous studies. (iii)

For the parameters subjected to calibration, physically, chemically, or biologically acceptable intervals for the parameter values are summarized in Table S5.

3.2. Data for model calibration and validation

Model calibration is to determine the appropriate values of selected parameters by achieving the best or acceptable goodness-of-fit between simulations and observations. Model validation is the process to demonstrate if a given model with the calibrated parameter values is capable of making good performance when a dataset independent of the calibration one is used [55, 56].

Generally, any observations of the state variables (Table S1: concentrations of C and N, and C:N ratios) and fluxes (Table S3 and S4) can be used for model calibration and validation. Traditional calibration and validation based on comparing simulated with observed total soil respiration or heterotrophic respiration still remains the only attainable option in many practical cases. However, this method is poorly consistent with microbe-explicit modeling. In addition to soil respiration (R_s), heterotrophic respiration (R_h), soil organic carbon (SOC), concentrations of soil available ammonium (NH_4^+) and nitrate (NO_3^-), and the rates of N fixation, nitrification, net N mineralization, and plant N uptake, microbial data should also be included in model calibration and validation where there are data available. For example, microbial biomass C and N, and omics-detected functional gene abundances.

Omics-detected gene abundances (GAs) data may be used for model calibration and/or validation depending on whether there are time-series data available. If there are multiple-time observations of GAs for the same functional gene, we may use them for model calibration and validation by estimating the correlation between omics-derived GAs and simulated enzyme concentrations (ECs), enzyme activities (EAs), or equivalent first-order reaction rates (FRs). As the Michaelis-Menten kinetics was used in the MEND model, the FR (h^{-1}) is defined as

$Vd \times E/(K+S)$, where S and E are the substrate concentration and the corresponding enzyme concentration (mg C cm^{-3} soil), respectively. The parameters V_d and K denote the specific enzyme activity (mg C mg^{-1} C h^{-1}) and the half-saturation constant (mg C cm^{-3}), respectively. The product of V_d and E represents the enzyme activity (mg C cm^{-3} h^{-1}). When observed response ratios (*RR*s) of GAs between different treatments (e.g., elevated versus ambient CO_2) are available, we may calibrate and/or validate the model by comparing omics-derived RRs of GAs and simulated RRs of ECs, EAs, or FRs. These enzymes (genes) mediate SOM decomposition and inorganic N transformations. In this study, we used the *RRs* for model evaluation.

3.3. Multi-objective parameter sensitivity analysis

Sensitivity analysis is used to identify important model parameters for model-data integration. We developed a Multi-Objective Parameter Sensitivity Analysis (MOPSA) method based on the Wilcoxon Rank Sum Test [57]. The MOPSA can be used to identify the relative importance of each model parameter for each objective or response variable (e.g., a C or N pool or flux). The sensitivity is characterized by the difference in the probability distribution between two (i.e., acceptable and unacceptable) parameter samples that are separated by a threshold of the objective functional values in terms of a specific response variable. The difference is statistically quantified by the Wilcox estimator from the non-parametric Wilcoxon Rank Sum Test, which is more applicable to statistical analysis of difference in parameters that are often not normally distributed [57]. This Wilcox estimator is then used as the sensitivity index to quantify the magnitude of parameter sensitivity, i.e., higher sensitivity index means higher sensitivity. Detailed description of the MOPSA procedure is presented in Supplementary Section 3.3.

The Wilcox-based Multi-Objective Parameter Sensitivity Analysis (MOPSA) approach consists of the following steps:

(i) Generating parameter samples. Select the parameters to be evaluated and generate parameter sets in terms of their ranges using the sample generator in the MOEA Framework [58].

(ii) Running MEND model to calculate objective function values. Run MEND with these parameter sets and compute the objective function values in terms of response variables (e.g., C or N pools or fluxes). The objective function is defined as the mean squared error (MSE) between simulated and reference time-series data. The simulated data are the simulated pool sizes or fluxes using a generated parameter set. the reference data refer to model-simulated pool sizes or fluxes using the medians of parameters.

(iii) Identifying acceptable and unacceptable parameter sets. For each response variable, identify whether a parameter set is acceptable or unacceptable by comparing the MSE to a given criterion, e.g., the 50% divisions of the sorted MSE. The MSE less than the criterion is classified as acceptable, otherwise it is classified as unacceptable.

(iv) Normalizing the parameter values by their value ranges. For the *i*th parameter, let $X_i = \{x_{i,j}, j = 1,2,\cdots,2n\}$ be the parameter values. Define $x_{i,\min} = \min\{X_i\}$ and $x_{i,\max} = \max\{X_i\}$, and the normalized X_i, denoted by $Z_i = \{z_{i,j}, j = 1,2,\cdots,2n\}$ is defined as $z_{i,j} = \frac{x_{i,j} - x_{i,\min}}{x_{i,\max} - x_{i,\min}} \in [0,1]$. Let $Z_i^A = \{z_{i,j}^A, j = 1,2,\cdots,n\}$ and $Z_i^U = \{z_{i,j}^U, j = 1,2,\cdots,n\}$ be the subsets of acceptable and unacceptable Z_i (i.e., normalized X_i), respectively. The normalization of parameter values makes the sensitivity index comparable between different parameters.

(v) Conducting the Wilcox test to determine parameter sensitivity. Implement the Wilcox test of the two parameter samples, i.e., Z_i^A and Z_i^U. The Wilcox estimator for the difference between acceptable and unacceptable parameters is used as the sensitivity index to quantify the magnitude of parameter sensitivity, i.e., higher sensitivity index means higher sensitivity. The *p-value* from the Wilcox test is used to evaluate if the parameter sensitivity is statistically significant (*p-value* <

0.05) or not (*p-value* ≥ 0.05). Note that the Wilcox estimator refers to the median of the difference between acceptable and unacceptable parameter samples [57].

3.4. Multi-objective Functions for model calibration and validation

We calibrate selected model parameters (Table S5) by achieving high goodness-of-fits of model simulations against experimental observations. We implement multi-objective calibration of the model [3, 4, 59]. Each objective evaluates the goodness-of-fit of a specific observed variable mentioned above. The parameter optimization is to minimize the overall objective function (*J*) that is computed as the weighted average of multiple single-objectives [56].

$$J = \sum_{i=1}^{m} w_i \cdot J_i \quad (67a)$$

$$\sum_{i=1}^{m} w_i = 1 \text{ and } w_i \in [0,1] \quad (67b)$$

where m denotes the number of objectives and w_i is the weighting factor for the i^{th} (i = 1,2,…, m) objective function (J_i).

The individual objective function J_i may be calculated as $(1- R^2)$, $|PBIAS|$, $MARE$, $MAREt$, or $(1-r)$:

$$R^2 = 1 - \frac{\sum_{i=1}^{n}[Y_{sim}(i)-Y_{obs}(i)]^2}{\sum_{i=1}^{n}[Y_{obs}(i)-\bar{Y}_{obs}]^2} \quad (68)$$

$$|PBIAS| = \left|\frac{\bar{Y}_{sim}-\bar{Y}_{obs}}{\bar{Y}_{obs}}\right| \quad (69)$$

$$MARE = \frac{1}{n}\sum_{i=1}^{n}\left|\frac{Y_{sim}(i)-Y_{obs}(i)}{Y_{obs}(i)}\right| \quad (70)$$

$$MAREt = \begin{cases} 0, & MARE \le tolerance \\ MARE, & MARE > tolerance \end{cases} \quad (71)$$

$$r = \frac{\sum_{i=1}^{n}[Y_{obs}(i)-\bar{Y}_{obs}]\cdot[Y_{sim}(i)-\bar{Y}_{sim}]}{\sqrt{\sum_{i=1}^{n}[Y_{obs}(i)-\bar{Y}_{obs}]^2}\cdot\sqrt{\sum_{i=1}^{n}[Y_{sim}(i)-\bar{Y}_{sim}]^2}} \quad (72)$$

where R^2 denotes the coefficient of determination; $|PBIAS|$ is the percent bias between simulated and observed mean values; $MARE$ is the Mean Absolute Relative Error (MARE) and represents

the averaged deviations of simulations (Y_{sim}) from their observations (Y_{obs}); *MAREt* is a variant of *MARE* and *MAREt* achieves the best (=0) when *MARE* is within a defined tolerance value; *r* is the Pearson correlation coefficient; *n* is the number of data; Y_{obs} and Y_{sim} are observed and simulated values, respectively; and $\bar{Y}_{obs}$ and $\bar{Y}_{sim}$ are the mean value for Y_{obs} and Y_{sim}, respectively.

Different objective functions are used to quantify the goodness-of-fit for different variables, depending on the measurement method and frequency of variables. R^2 quantifies the proportion of the variance in the response variables that is predictable from the independent variables [4]. A higher R^2 ($R^2 \leq 1$) indicates better model performance. R^2 is used to evaluate the variables (e.g., total soil respiration or heterotrophic respiration) that are frequently measured, and the absolute values can be directly compared between observations and simulations. *MARE* or |*PBIAS*| is used to evaluate the variables (e.g., microbial biomass C and concentrations of inorganic N) with only a few measurements and the absolute values can be directly compared. Lower *MARE* or |*PBIAS*| values (≥ 0) are preferred [4, 60]. *MAREt* should be used when the simulated value may not be necessarily to strictly match the observed or measured value. For example, the measured nitrification rates are more like potential rates or rough estimates. It is more appropriate to use *MAREt* to evaluate the model simulated actual nitrification rates when compared with these measurements. Another example includes the comparison between simulated and observed N fixation or plant N uptake rates. The observations collected from literature just represent empirical or reference N fixation [61] or plant N uptake rates [62, 63]. In this case, we also recommended to use *MAREt* as we expected the simulated N fixation or plant N uptake rates would fall into the observed value ranges. When the absolute values between simulations and observations cannot be directly compared, the correlation coefficient (*r*) between original or transformed (e.g., logarithmic transformed) observations and simulations will be used. For example, the gene abundances from

omics analysis cannot be directly compared to the enzyme concentrations or activities in the MEND model. However, we may assume correlation could be found between the measured and modeled values with a certain transformation or normalization. Noting that the coefficient of determination (R^2) is simply the square of the correlation coefficient (r) in case of a linear regression with an intercept. In other cases, e.g., a linear regression without including an intercept or a nonlinear fitting, R^2 may not be equivalent to r^2.

3.5. Model parameter calibration (optimization) algorithm

We use the modified Shuffled Complex Evolution (SCE) algorithm [59, 64, 65] to calibrate selected model parameters by minimize the overall objective function (J) as shown in Eq. 67a. SCE is a stochastic optimization method that includes competitive evolution of a 'complex' of points spanning the parameter space and the shuffling of complexes [59]. SCE has been widely used in calibration of hydrological, environmental, and ecosystem models and proved to be efficient and robust [3, 60, 66-68].

3.6. Uncertainty quantification

The uncertainties in parameters and model predictions are evaluated by the Uncertainty Quantification by Critical Objective Function Index (UQ-COFI) method [3], which is much simpler than the commonly used method based on Bayesian inference and Markov Chain Monte Carlo (MCMC) [37]. The UQ-COFI method is based on a global stochastic optimization technique (e.g., SCE in this study). It also accounts for model complexity (represented by the number of model parameters) and observational data availability (represented by the number of observations). The confidence region of parametric space were determined by selecting those parameter sets

resulting in objective function values (J) less than the COFI value (J_{cr}) from the feasible parameter space [3]. The COFI (J_{cr}) is defined as [3, 69]:

$$J_{cr} = J_{opt} \cdot \eta = J_{opt} \cdot \left(1 + \frac{p}{n-p} \cdot F_{\alpha,p,n-p}\right) \quad (73)$$

where J_{cr} is the COFI that defines the parameter uncertainty region, J_{opt} is the optimum (minimum) objective function value that is calculated by Eq. 2, n is the number of measured data points, p is the number of parameters, and $F_{\alpha,p,n-p}$ is the value of the F-distribution for α, p, and $n-p$. It is evident that more observed data points (i.e., larger n) and less undetermined parameters (i.e., smaller p) would reduce parametric uncertainty (i.e., lower J_{cr}).

The procedure of UQ-COFI includes: (i) implementing the SCE algorithm with multiple different random seeds to search 'relatively optimal' parameter sets that minimizing the objective function (J in Eq. 67a); (ii) collecting the optimal parameter set generated in each loop of the SCE searching process to form a feasible parameter space; (iii) determining the critical objective function index (COFI) (J_{cr}) (see Eq. 8 in main text) based on J_{opt} (minimum J value), n (number of measurements) and p (number of model parameters); (iv) constructing the parametric surface of the confidence space by selecting those parameter sets resulting in $J \leq J_{cr}$ from the feasible parameter space; (v) quantifying the uncertainty in parameters by the statistics of these selected parameter sets; (vi) conducting model simulations using these selected parameter sets; and (vii) quantifying the uncertainty in model predictions (e.g., soil C pool sizes and respiration) using the model simulation outputs.

4. Supplementary Tables

Table S1. Soil carbon (C) and nitrogen (N) pools (state variables) in the MEND model

ID	Soil C and/or N pool	Pool Name	Variable name
1	Particulate organic matter (POM) decomposed by oxidative enzymes	POM_O	C pool: *PO*; N pool: *PON*
2	POM decomposed by hydrolytic enzymes	POM_H	*PH*; *PHN*
3	Mineral-associated organic matter	MOM	*M*; *MN*
4	Dissolved organic matter	DOM	*D*; *DN*
5	Active MOM interacting with DOM	QOM	*Q*; *QN*
6	Active microbial biomass	MB_A	*BA*; *BAN*
7	Dormant microbial biomass	MB_D	*BD*; *BDN*
8	Oxidative enzymes decomposing POM_O	EP_O	*EPO*; *EPON*
9	Hydrolytic enzymes decomposing POM_H	EP_H	*EPH*; *EPHN*
10	Enzymes decomposing MOM	EM	*EM*; *EMN*
11	Ammonium oxidase	ENH4	*ENH4*; *ENH4N*
12	Nitrate reductase	ENO3	*ENO3*; *ENO3N*
13	Nitrite reductase	ENO2	*ENO2*; *ENO2N*
14	Nitric oxide reductase	ENO	*ENO*; *ENON*
15	Nitrous oxide reductase	EN2O	*EN2O*; *EN2ON*
16	Nitrogenase	EN2	*EN2*; *EN2N*
17	Adsorbed ammonium	NH_4^+ Adsorb	*NH4ads*
18	Ammonium	NH_4^+	*NH4*
19	Nitrate	NO_3^-	*NO3*
20	Nitrite	NO_2^-	*NO2*
21	Nitric oxide	NO	*NO*
22	Nitrous oxide	N_2O	*N2O*
23	Dinitrogen	N_2	*N2*

Table S2. Governing equation for each soil C or N pool (Table S1) in the MEND model

Governing Equation	Eq#
Soil Carbon (state variable, e.g., *PH*, denotes the C content in POM_H pool)**:**	
$dPO/dt = I_{PO} + (1-g_D)\cdot g_{PO}\cdot F_9 - F_1$; $I_{PO} + I_{PH} + I_D = I_{gross}\cdot fINP$; I_{gross} is gross litter input	(1)
$dPH/dt = I_{PH} + (1-g_D)\cdot(1-g_{PO})\cdot F_9 - F_2$	(2)
$dM/dt = (1-f_D)\cdot(F_1+F_2) - F_3$	(3)
$dQ/dt = F_4 - F_5$	(4)
$dD/dt = I_D + f_D\cdot(F_1+F_2) + F_3 + g_D\cdot F_9 + F_{16} - F_6 - (F_4 - F_5)$	(5)
$dBA/dt = F_6 - (F_7 - F_8) - F_9 - (F_{10}+F_{11}+F_{12}) - (F_{15}+F_{17}) + F_{18}$	(6)
$dBD/dt = (F_7 - F_8) - (F_{13}+F_{14})$	(7)
$dED_i/dt = F_{15,ED_i} - F_{16,ED_i}$; ED_i $(i = 1,2,3)$ denotes *EPO*, *EPH*, *EM*, respectively	(8)
$dEN_j/dt = F_{17,EN_j} - F_{18,EN_j}$; EN_j $(j = 1,2,\cdots,6)$ denotes *ENH4*, *ENO3*, *ENO2*, *ENO*, *EN2O*, *EN2*, respectively	(9)
$R_h = (F_{10}+F_{11}+F_{12}) + (F_{13}+F_{14})$; heterotrophic (microbial) respiration	(10)
$R_a = fR_a\cdot GPP$; autotrophic (root) respiration	(11)
$R_s = R_a + R_h$; total soil respiration	(12)
$\frac{d}{dt}\left(PO + PH + M + Q + D + BA + BD + \sum_{i=1}^{3} ED_i + \sum_{j=1}^{6} EN_i\right) = (I_{PO} + I_{PH} + I_D) - R_h$	(13)
Soil Nitrogen (state variable, e.g., *PHN*, denotes the N content in POM_H pool)**:**	
• For soil organic matter pools, the *N* flux: $FN_k = F_k/CN_{source}$, where F_k (k = 1–9) is the *C* flux, and CN_{source} is the C:N ratio of the (upstream) source pool.	(14a)
• For enzymes pools ED_i $(i = 1,2,3)$ and EN_j $(j = 1,2,\cdots,6)$, the *N* flux $FN_k = F_k/CN_{ENZ}$, k = 15–18.	(14b)
$\frac{dBAN}{dt} = \frac{F_6}{CN_D} - \left(\frac{F_7}{CN_{BA}} - \frac{F_8}{CN_{BD}}\right) - \frac{F_9}{CN_{BA}} - \frac{F_{15}+F_{17}}{CN_{ENZ}} + \frac{F_{18}}{CN_{ENZ}} - FN_{mn,BA} + \left(FN_{im,NH4\to BA} + FN_{im,NO3\to BA}\right)$	(15)
$dBDN/dt = (F_7/CN_{BA} - F_8/CN_{BD}) - FN_{mn,BD}$	(16)
$dNH4/dt = I_{NH4} + FN_{fix} + \left(FN_{mn,BA} + FN_{mn,BD}\right) - \left(FN_{im,NH4\to BA} + FN_{im,NH4\to VG}\right) - FN_{nit}$	(17)
$dNO3/dt = I_{NO3} + FN_{nit} - FN_{nit-denit} - FN_{denit_2} - \left(FN_{im,NO3\to BA} + FN_{im,NO3\to VG}\right) - FN_{leach,NO3}$	(18)
$dNO2/dt = FN_{denit_2} - FN_{denit_3} - FN_{leach,NO2}$	(19)
$dNO/dt = FN_{denit_3} - FN_{denit_4} - FN_{emit_4}$	(20)
$dN2O/dt = FN_{nit-denit} + FN_{denit_4} - FN_{denit_5} - FN_{emit_5}$	(21)
$dN2/dt = FN_{denit_5} - FN_{fix} - FN_{emit_6}$	(22)
$\frac{d}{dt}\left(PON + PHN + MN + QN + DN + BAN + BDN + \sum_{i=1}^{3} EDN_i + \sum_{j=1}^{6} ENN_i\right) = (IN_{PO} + IN_{PH} + IN_D) + \left(FN_{im,NH4\to BA} + FN_{im,NO3\to BA}\right) - \left(FN_{mn,BA} + FN_{mn,BD}\right)$	(23a)
$\frac{d}{dt}\left(NH4ads + \sum_{j=1}^{6} N_j\right) = (I_{NH4} + I_{NO3}) + \left(FN_{mn,BA} + FN_{mn,BD}\right) - \left(FN_{im,NH4\to BA} + FN_{im,NO3\to BA}\right) - \left(FN_{im,NH4\to VG} + FN_{im,NO3\to VG}\right) - \left(FN_{leach,NO3} + FN_{leach,NO2}\right) - \sum_{j=4}^{6} NF_{emit_j}$	(23b)
$\frac{d}{dt}\left(PON + PHN + MN + QN + DN + BAN + BDN + \sum_{i=1}^{3} EDN_i + \sum_{j=1}^{6} ENN_i + \sum_{j=1}^{6} N_j + NH4ads\right) = (IN_{PO} + IN_{PH} + IN_D) + (I_{NH4} + I_{NO3}) - \left(FN_{im,NH4\to VG} + FN_{im,NO3\to VG}\right) - \left(FN_{leach,NO3} + FN_{leach,NO2}\right) - \sum_{j=4}^{6} NF_{emit_j}$	(23c)

Note: Eqs. 13, 23a, 23b and 23c express the overall mass balance of soil organic C (SOC), soil organic N (SON), inorganic N and total N, respectively. The transformation fluxes (*F* or *FN*) are described in Table S3 and Table S4.

Table S3 Component fluxes in the MEND model (SOM decomposition, microbial and enzyme fluxes)

Flux description	Equation	Eq#
Particulate organic matter (POM) pool (oxidative) (*PO*) decomposition (F_1)	$F_1 = Vd_{PO} \cdot EPO \cdot PO/(K_{PO} + PO)$	(24)
POM pool (hydrolytic) (*PH*) decomposition	$F_2 = Vd_{PH} \cdot EPH \cdot PH/(K_{PH} + PH)$	(25)
Mineral-associated organic matter (*M*) decomposition	$F_3 = Vd_M \cdot EM \cdot M/(K_M + M)$	(26)
Adsorption (F_4) and desorption (F_5) between dissolved organic matter (*D*) and adsorbed DOM (*Q*)	$F_4 = k_{ads} \cdot (1 - Q/Q_{max}) \cdot D$ $F_5 = k_{des} \cdot (Q/Q_{max})$ $K_{ads} = K_{des} \cdot K_{ba}$	(27) (28)
DOM (*D*) uptake by microbes	$F_6 = \frac{1}{Y_g}(V_g + V_m) \cdot \frac{BA \cdot D}{K_D + D}$	(29)
Dormancy (F_7) and resuscitation (F_8) between active (*BA*) and dormant (*BD*) microbes	$F_7 = [1 - D/(K_D + D)] \cdot V_m \cdot BA$ $F_8 = [D/(K_D + D)] \cdot V_m \cdot BD$	(30) (31)
MB_A (*BA*) mortality	$F_9 = \gamma \cdot V_m \cdot BA$	(32)
MB_A (*BA*) growth respiration (F_{10}) and maintenance respiration (F_{11})	$F_{10} = \left(\frac{1}{Y_g} - 1\right) \cdot \frac{V_g \cdot BA \cdot D}{K_D + D}$ $F_{11} = \left(\frac{1}{Y_g} - 1\right) \cdot \frac{V_m \cdot BA \cdot D}{K_D + D}$	(33) (34)
MB_A (*BA*) overflow respiration (F_{12})	$F_{12} = max\{0, BA - BAN \cdot CN_{BA,max}\}$	(35)
MB_D (*BD*) maintenance respiration (F_{13})	$F_{13} = \beta \cdot V_m \cdot BD$	(36)
MB_D (*BD*) overflow respiration (F_{14})	$F_{14} = max\{0, BD - BDN \cdot CN_{BA,max}\}$	(37)
Synthesis of enzymes for decomposition of *PO* ($F_{15,EPO}$, $EPO = ED_1$), *PH* ($F_{15,EPH}$, $EPH = ED_2$), and *M* ($F_{15,EM}$, $EM = ED_3$)	$F_{15,EPO} = PO/(PO + PH) \cdot p_{EP} \cdot V_m \cdot BA$ $F_{15,EPH} = PH/(PO + PH) \cdot p_{EP} \cdot V_m \cdot BA$ $F_{15,EM} = fp_{EM} \cdot p_{EP} \cdot V_m \cdot BA$ $F_{15} = \sum_{i=1}^{3} F_{15,ED_j} = F_{15,EPO} + F_{15,EPH} + F_{15,EM}$	(38)
Turnover of enzymes ($EPO = ED_1$, $EPH = ED_2$, $EM = ED_3$)	$F_{16,ED_i} = r_E \cdot ED_i$ $F_{16} = \sum_{i=1}^{3} F_{16,ED_j}$	(39)
Synthesis of enzymes for nitrification, denitrification, and N fixation; EN_j ($j = 1-6$): *ENH4*, *ENO3*, *ENO2*, *ENO*, *EN2O*, *EN2*; N_j ($j = 1-6$): *NH4*, *NO3*, *NO2*, *NO*, *N2O*, *N2*; SON_i ($i = 1-5$): *PON*, *PHN*, *MN*, *QN*, *DN*	$F_{17} = \sum_{j=1}^{6} F_{17,EN_j} = F_{15} \cdot (NH4 + NO3 + NO2)/\sum_{i=1}^{4} SON_i$ $F_{17,EN_j} = \frac{N_j/KSN_j}{\sum_{j=1}^{6}(N_j/KSN_j)} \cdot F_{17}$	(40)
Turnover of enzymes for nitrification, denitrification, and N fixation	$F_{18} = \sum_{j=1}^{6} F_{18,EN_j}$; $F_{18,EN_j} = r_E \cdot EN_j$	(41)

Note: Model parameters are described in Table S5.

Table S4 Component fluxes in the MEND model (nitrification, denitrification, N fixation, N mineralization and immobilization, NH_4^+ sorption, NO_3^- and NO_2^- leaching, and N gases emission)

Flux description	Equation	Eq#
Nitrification	$FN_{nit} = \frac{VN_{nit} \cdot ENH4 \cdot NH4}{KSN_1 + NH4}$	(42)
Nitrifier Denitrification	$FN_{nit-denit} = FN_{nit} \cdot [1 - f(O_2)]$ $f(O_2) = \frac{(1-WFP)^{4/3}}{0.5^{4/3}+(1-WFP)^{4/3}}$; *WFP* is water-filled porosity	(43a) (43b)
Denitrification of *NO3*, *NO2*, *NO*, *N2O*: $j = 2,3,4,5$	$FN_{denit_j} = \frac{VN_j \cdot EN_j \cdot N_j}{KSN_j + N_j}$	(44)
N fixation	$FN_{fix} = \frac{VN_{fix} \cdot EN2 \cdot N2}{KSN_6 + N2} \cdot \left(1 - \frac{NH4}{KSN_1 + NH4}\right)$	(45)
N mineralization	$FN_{mn,BA} = (1 - YN_g) \cdot FN_6$ $YN_g = \left(\frac{CN_{BA} - CN_{BA,min}}{CN_{BA,max} - CN_{BA,min}}\right)^{\omega}$	(46) (47)
N immobilization by microbes	$FN_{im,NH4\rightarrow BA} = \left[\left(VN_{im,NH4} \cdot YN_g\right) \cdot BA \cdot NH4\right]/(KSN_{BA1} \cdot \eta)$ $FN_{im,NO3\rightarrow BA} = \left[\left(VN_{im,NO3} \cdot YN_g\right) \cdot BA \cdot NO3\right]/(KSN_{BA2} \cdot \eta)$ $\eta = 1 + \frac{BA}{KSN_{BA1}} + \frac{NH4}{KSN_{BA1}} + \frac{NO3}{KSN_{BA2}} + \frac{NH4}{KSN_{VG1}} + \frac{NO3}{KSN_{VG2}}$	(48) (49) (50)
N uptake by plants	$FN_{im,NH4\rightarrow VG} = \left[\left(VN_{VG,NH4} \cdot rGPP\right) \cdot NH4\right]/(KSN_{VG1} \cdot \eta)$ $FN_{im,NO3\rightarrow VG} = \left[\left(VN_{VG,NO3} \cdot rGPP\right) \cdot NO3\right]/(KSN_{VG2} \cdot \eta)$ Coefficient *rGPP* = *f*(GPP), e.g., $rGPP = \exp\left[\omega_{VG} \cdot \left(GPP/GPP_{ref} - 1\right)\right]$	(51) (52)
NH_4^+ sorption	$NH4 = \left[A + \sqrt{A^2 + 4K_{ba,NH4} \cdot NH4tot}\right]/(2 \cdot K_{ba,NH4})$ $NH4ads = NH4tot - NH4$ where $A = K_{ba,NH4} \cdot (NH4tot - NH4_{max}) - 1$ derived from: $NH4ads + NH4 = NH4tot$ $NH4ads = NH4_{max} \cdot \left(K_{ba,NH4} \cdot NH4\right)/(1 + K_{ba,NH4} \cdot NH4)$	(53a) (53b) (53c) (53d) (53e)
NO_3^- and NO_2^- leaching	$FN_{leach,NO3} = NO3 \cdot fN_{leach}$ $FN_{leach,NO2} = NO2 \cdot fN_{leach}$ where: $fN_{leach} = r_{leach} \cdot fN_{dissolved} \cdot \left(\theta_{perc}/\theta\right)$ $fN_{dissolved} = (\theta/\theta_{sat})^3$ $\theta_{perc} = \theta_{excess} \cdot \left[1 - \exp\left(-\Delta t/TT_{perc}\right)\right]$ $\theta_{excess} = \max(0, \theta - \theta_{FC})$ $TT_{perc} = (\theta_{sat} - \theta_{FC}) \cdot Depth/K_{sat}$ $r_{leach} \in (0,1)$: scaling factor; θ: volumetric soil water content (SWC); θ_{sat} and θ_{FC}: SWC at saturation and field capacity; *Depth*: soil depth (cm); θ_{excess}: excess SWC available for percolation; θ_{perc}: SWC percolation; K_{sat}: saturated hydraulic conductivity (cm h^{-1}); Δt: given time-period (= 1h); TT_{perc}: travel time for percolation (h)	(54a) (54b) (54c) (54d) (54e) (54f) (54g)
NO, N_2O, N_2 gas emission: j = 4,5,6	$FN_{emit_j} = \left[Ds_j \cdot \left(N_j - Nair_j\right)/(0.5 \cdot Depth)\right]/Depth$ where: Ds_j: gas diffusivity in soil (cm^2 h^{-1}); N_j and $Nair_j$ gas concentration in soil and air (mg N cm^{-3})	(55)

Note: Model parameters are described in Table S5.

Table S5 MEND model parameters

ID	Parameter	Description	Range	Units	Eq#
1	LF_0	Initial fraction of *PO*, $LF_0 = PO/(PO+PH)$	(0.1, 1.0)	—	
2	r_0	Initial active fraction of microbes, $r_0 = BA/(BA+BD)$	(0.01, 1)	—	
3	fR_a	Scaling factor for autotrophic respiration (R_a)	(0.1, 0.4)	—	11
4	$fINP$	Scaling factor for litter input rate	(0.1, 0.9)	—	1
5	Vd	Maximum specific decomposition rate $Vd_{PO} = Vd_{PH} = Vd_M = Vd$	(0.1, 100)	mg C mg^{-1} C h^{-1}	24–26
6	K_{PO}	Half-saturation constant (HSC) for *PO* decomposition	(40,100)	mg C cm^{-3} soil	24
7	fK_M	$K_M = K_{PO} \times fK_M$, $K_{PH} = K_{PO}/fK_M$ K_{PH} and K_M are HSC for *PH* and *M*, respectively	(2, 20)	—	25–26
8	Q_{max}	Maximum sorption capacity	(0.5, 5.0)	mg C cm^{-3} soil	27
9	K_{ba}	Binding affinity for DOM, sorption rate $k_{ads} = k_{des} \times K_{ba}$	(1, 16)	(mg C cm^{-3} soil)$^{-1}$	27
10	k_{des}	Desorption rate for DOM	(1e-4, 0.01)	mg C cm^{-3} soil h^{-1}	28
11*	r_E	Enzyme turnover rate	(1e-4, 0.01)	mg C mg^{-1} C h^{-1}	39, 41
12*	p_{EP}	$[V_m \times p_{EP}]$ is the production rate of *EP* (*EPO* + *EPH*), V_m is the specific maintenance rate for *BA*	(1e-3, 0.1)	—	38
13*	fp_{EM}	$fp_{EM} = p_{EM}/p_{EP}$, $[V_{mt} \times p_{EM}]$ is the production rate of *EM*	(0.1, 5.0)	—	38
14	f_D	Fraction of decomposed *PO* and *PH* allocated to *D*	(0.05, 1)	—	3
15	g_D	Fraction of dead *BA* allocated to *D*	(0.01, 1)	—	1
16	g_{PO}	$(1 - g_D) \cdot g_{PO}$ is the fraction of dead *BA* entering *PO*	(0.05, 0.2)	—	2
17*	V_g	Maximum specific uptake rate of *D* for growth	(1e-3, 0.1)	mg C mg^{-1} C h^{-1}	29
18*	α	$= V_m / (V_g + V_m)$, V_m is max specific maintenance rate	(0.01, 0.5)	—	29
19*	K_D	HSC for microbial uptake of *D*	(1e-4, 0.5)	mg C cm^{-3} soil	29
20*	$Y_g(T_{ref})$	Intrinsic C use efficiency at reference temperature (T_{ref})	(0.2, 0.4)	—	29
21*	kY_g	Slope for Y_g dependence of temperature	(1e-3, 0.016)	1/°C	29
22	Q_{10}	Q_{10} for temperature response function	(1.2, 2.5)	—	
23*	γ	Max microbial mortality rate = $V_m \times \gamma$	(0.01, 20)	—	32
24	β	Ratio of dormant maintenance rate to V_m	(5e-4, 0.05)	—	36
25	ψ_{A2D}	Soil water potential (SWP) threshold for microbial dormancy; both ψ_{A2D} & $\psi_{D2A} < 0$	(–0.6, –0.2)	MPa	
26	τ	$\psi_{D2A} = \psi_{A2D} \times \tau$, ψ_{D2A} is the SWP threshold for microbial resuscitation	(0.1, 0.9)	—	
27	ω	Exponential in SWP function for microbial dormancy or resuscitation	(1, 6)	—	
28*	$VN_{im,BA}$	Max specific microbial N immobilization rate $VN_{im,NH4} = VN_{im,BA} \cdot NH4/(NH4 + NO3)$ $VN_{im,NO3} = VN_{im,BA} \cdot NO3/(NH4 + NO3)$	(1e-4, 0.1)	mg N mg^{-1} C h^{-1}	48, 49
29	KSN_{BA1}	HSC for microbial immobilization of NH_4^+	(1e-4, 0.01)	mg N cm^{-3} soil	48–50
30	KSN_{BA2}	HSC for microbial immobilization of NO_3^-	(1e-4, 0.01)	mg N cm^{-3} soil	48–50
31*	VN_{nit}	Max specific nitrification rate (VN_1)	(0.1, 1000)	mg N mg^{-1} C h^{-1}	42
32*	VN_{denit}	Max specific denitrification rate, $VN_j = VN_{denit}$, j=2–5	(1e-4, 1.0)	mg N mg^{-1} C h^{-1}	44
33*	VN_{fix}	Max specific N fixation rate (VN_6)	(1e-4, 0.1)	mg N mg^{-1} C h^{-1}	45
34	KSN_1	HSC for nitrification	(1e-3, 1.0)	mg N cm^{-3} soil	42
35	KSN_2	HSC for denitrification of NO_3^- and NO_2^- (KSN_3)	(1e-4, 0.1)	mg N cm^{-3} soil	44
36	KSN_4	HSC for denitrification of NO and N_2O (KSN_5)	(1e-4, 0.1)	mg N cm^{-3} soil	44
37	KSN_6	HSC for N fixation	(1e-4, 0.1)	mg N cm^{-3} soil	45
38*	VN_{VG}	Max plant N uptake rate; $VN_{VG,NH4} = VN_{VG,NO3} = VN_{VG}$	(1e-6, 1e-3)	mg N cm^{-3} h^{-1}	51, 52
39	KSN_{VG1}	HSC for plant uptake of NH_4^+	(1e-4, 0.01)	mg N cm^{-3} soil	51
40	KSN_{VG2}	HSC for plant uptake of NO_3^-	(1e-4, 0.01)	mg N cm^{-3} soil	52
41	ω_{VG}	Exponential for calculating *rGPP* as a function of GPP	(0.01, 1)	—	52
42*	$NH4_{max}$	Maximum sorption capacity for NH_4^+	(1e-5, 0.01)	mg N cm^{-3} soil	53
43	$K_{ba,NH4}$	Binding affinity for NH_4^+	(1, 1e4)	(mg N cm^{-3} soil)$^{-1}$	53
44	r_{leach}	Scaling factor for NO_3^- and NO_2^- leaching	(0.01, 1)	—	54

Notes: '*' in the column 'ID' denotes the parameters calibrated in this study. The column 'Eq#' lists the major equation # where each parameter is used.

Table S6 MEND model: response functions of soil pH, temperature, and moisture

Function description	Response function	Variables and Parameters	Eq#
Reaction rate	$v = v_0 \cdot f(\psi) \cdot f(T) \cdot f(pH)$ $f(\psi)$: soil moisture response function (SMRF) $f(T)$: soil temperature response function; $f(pH)$: pH response function	v_0: baseline reaction rate; ψ: soil water potential, SWP (MPa); T: soil temperature; pH: soil pH	56
Soil pH response function	$f(pH) = exp\left[-\left(\frac{pH - pH_{opt}}{pH_{sen}}\right)^2\right]$	pH_{opt}: optimum pH that gives the maximum reaction rate; pH_{sen}: sensitivity of the reaction rate to deviation from pH_{opt}	57
Temperature sensitivity of intrinsic carbon use efficiency (Y_g)	$Y_g(T) = Y_g(T_{ref}) - k_{Yg} \cdot (T - T_{ref})$	$Y_g(T_{ref})$: Y_g at reference temperature, T_{ref} (°C); $-k_{Yg}$: the slope, –0.016 ≤ $-k_{Yg}$ ≤ –0.001 °C $^{-1}$	58
Temperature response: Arrhenius equation or Q_{10} method	$f(T) = exp\left[-\frac{Ea}{R}\left(\frac{1}{T} - \frac{1}{T_{ref}}\right)\right]$ $f(T) = Q_{10}^{\frac{T - T_{ref}}{10}}$ $Q_{10} = exp\left[\frac{Ea}{R \cdot T_{ref}} \cdot \frac{10}{T}\right]$	T: temperature (K); T_{ref}: reference temperature (K); Ea: activation energy (kJ mol^{-1}); R = 8.314 J mol^{-1} K^{-1}, the universal gas constant; Q_{10}: the factor by which the reaction rate is multiplied when temperature increases over T_{ref} by 10 K	59 60 61
SMRF for SOM decomposition by oxidative enzymes	$f_{oxi}(\psi) = \begin{cases} 0, & \psi \le -10^{2.5} \\ 0.625 - 0.25 \times \log_{10}(-\psi), & -10^{2.5} < \psi \le -10^{1.5} \\ 1, & -10^{1.5} < \psi \le -10^{-2.5} \\ [2.5 + 0.4 \times \log_{10}(-\psi)]/1.5, & -10^{-2.5} < \psi \le -10^{-4} \\ 0.6, & \psi > -10^{-4} \end{cases}$	ψ: soil water potential (MPa) Hansen et al. [45]	62
SMRF for SOM decomposition by hydrolytic enzymes	$f_{hyd}(\psi) = \begin{cases} 0, & \psi \le \psi_{min} \\ 1 - \left[\frac{\ln(\psi/\psi_{FC})}{\ln(\psi_{min}/\psi_{FC})}\right]^b, & \psi_{min} < \psi \le \psi_{FC} \\ 1, & \psi > \psi_{FC} \end{cases}$	ψ: soil water potential (MPa); ψ_{FC}= −0.033 MPa: SWP at field capacity; ψ_{min}: microbial stress threshold SWP; b: a shape parameter Manzoni *et al*. [46]	63
SMRF for microbial dormancy & resuscitation	$f_{A2D}(\psi) = \frac{1}{1 + [\psi_{A2D}/\psi]^\omega}$ $f_{D2A}(\psi) = \frac{1}{1 + (\psi/\psi_{D2A})^\omega} = \frac{1}{1 + [\psi/(\psi_{A2D} \times \tau)]^\omega}$	ψ: soil water potential (MPa); ψ_{A2D} (MPa): critical SWP for microbial dormancy; ψ_{D2A} (MPa): critical SWP for microbial resuscitation; $\tau = \psi_{D2A}/\psi_{A2D}$; ω: exponent to describe the steepness of the curve	64 65
SMRF for nitrification & denitrification	$f(WFP) = \begin{cases} 0 & WFP \le WFP_1 \\ a_+ + b_+ \cdot WFP & WFP_1 < WFP \le WFP_2 \\ 1 & WFP_2 < WFP \le WFP_3 \\ a_- + b_- \cdot WFP & WFP_3 < WFP \le WFP_4 \\ 0 & WFP > WFP_4 \end{cases}$	$WFP = \theta/\phi$: water-filled pore space; θ: volumetric water content; ϕ soil porosity; a_+ and b_+ are intercept and slope of linear regression for increasing activity (i.e., $b_+ > 0$); a_- and b_- are intercept and slope of linear regression for decreasing activity (i.e., $b_- < 0$); $WFP_i, (i = 1,2,3,4)$ and a_+, b_+, a_-, b_- are adapted from Muller [48].	66

5. Supplementary Results

5.1. MEND parameter sensitivity

Based on the MOPSA approach, we summarized the sensitivity of 13 major C and N variables to 36 model parameters in MEND-new (Supplementary Fig. S5). The sensitivity indices ranged from 0 to 0.29, where a greater value means a higher sensitivity. We used the cutoff value of 0.05 for sensitivity indices to distinguish important from unimportant parameters, as 0.05 denoted small difference when all parameter values were normalized to the range between 0 and 1.

Our MOPSA results show that most of the sensitivity indices were below 0.05 (gray and white colors), though most differences were statistically significant (gray colors with p-value < 0.05). Soil organic matter pools (SOM, POM, MOM, and DOM) and microbial pools (MB, MB_A, and MB_D) were more sensitive to microbial physiological parameters (e.g., specific growth rate (V_g), maintenance rate (controlled by α), intrinsic C use efficiency (Y_g), and the temperature sensitivity of Y_g (kY_g)) than those parameters regulating inorganic N transformations (i.e., from microbial N immobilization rate ($VNim_{MB}$) to binding affinity for NH_4^+ adsorption (Kba_{NH4})). Enzymes (ENZ_{SOM} for SOM decomposition and ENZ_{Nmin} for inorganic N transformations) were majorly regulated by enzyme production and turnover (p_{EP}, fp_{EM}, fp_{ENZN}, and r_E) as well as microbial maintenance (controlled by α). The parameters governing biological N fixation (e.g., VN_{fix}) and plant N uptake (e.g., VN_{plant}) were more influential on the inorganic N pools (NH_4^+, NO_3^-, and N_2O), so were the parameters related to enzyme production and turnover (p_{EP} and r_E), and microbial growth and maintenance (V_g and α). The cutoff threshold of 0.05 to separate important from unimportant parameters in this study is also frequently accepted in the Sobol sensitivity analysis to identify important parameters [58]. Moving the cutoff value would affect the number of important parameters (Fig. S5).

The sensitivity analysis results shown in Fig. S5 provided favorable guidance on the MEND model calibration: (i) we could use a two-step procedure to calibrate model parameters, with the first step focusing on SOM and microbial physiological parameters (i.e., from specific enzyme activity (V_d) to dormant microbial maintenance coefficient (β)) and the second step on inorganic N parameters (i.e., from $VNim_{MB}$ to Kba_{NH4}); (ii) in each calibration step, we could select the most important (i.e., sensitive) parameters to calibrate against relevant observations, with the other less important or well-documented parameters being fixed.

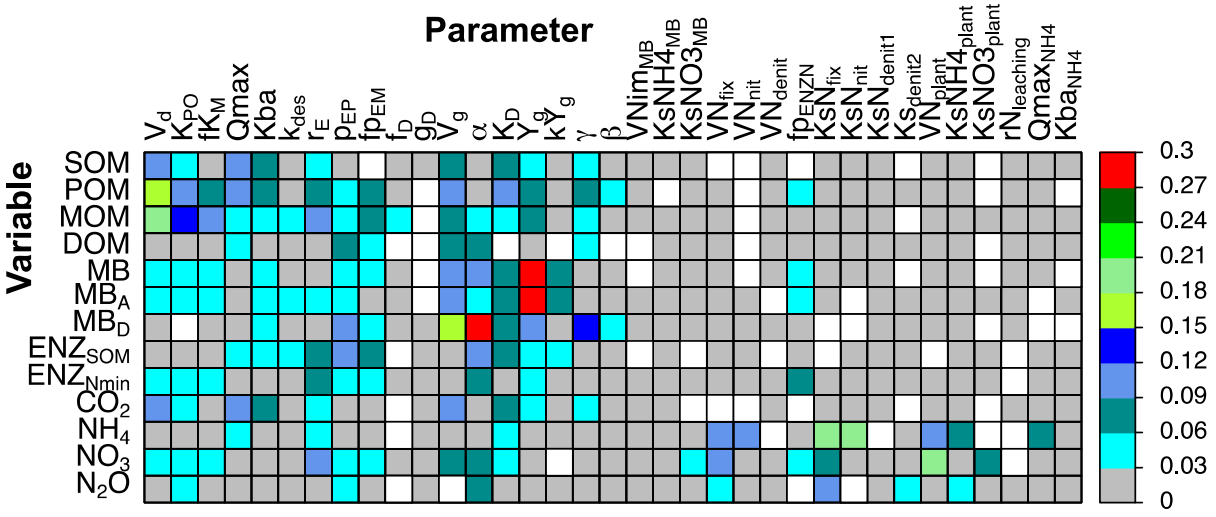

Figure S5. MEND parameter sensitivity analysis. Variables and parameters were described in Supplementary Table S1 and S5, respectively. ENZ_{SOM} denotes the total concentrations of three functional enzyme groups for soil organic matter decomposition. ENZ_{Nmin} represents the total concentrations of six enzyme groups for inorganic N transformations. The sensitivity index is defined as the median of the difference between acceptable and unacceptable parameter samples identified by the Multi-Objective Parameter Sensitivity Analysis (MOPSA) method. A higher sensitivity index means the variable is more sensitive to that parameter. Sensitivity indices are statistically significant (*p-value* < 0.05) except for those grids in white color (*p-value* ≥ 0.05) according to the Wilcoxon Rank Sum Test.

5.2. Quantification of uncertainties in parameters and response variables

Using the UQ-COFI method, we derived the posteriori distributions of 14 calibrated parameters (Supplementary Fig. S6) from the *a priori* uniform distributions within their respective parameter range (Supplementary Table S5). None of the 14 parameters conformed to a normal or log-normal distribution (p-value < 0.001) by the Anderson-Darling normality test [70], consistent with the observation that ecological data may not be normally distributed [70]. Averagely, the 95% confidence intervals of the posteriori parameters shrank to around 43% of the original *a priori* ranges.

The uncertainties in response variables were also evaluated by running the model with these posteriori parameter sets. For example, the 95% confidence intervals of simulated R_s due to parameter uncertainty expanded from 4% to 297% (averagely 50%) of the observed standard deviations, and the ratios of simulated to observed standard deviations ranged from 1% to 87% with an average of 13% (Fig. 3a). Note that parameter uncertainty was solely considered in these model simulations. It implies that the uncertainty in measured data (e.g., R_s in this study) could be another important source for uncertainty analysis in model-data integration studies [71].

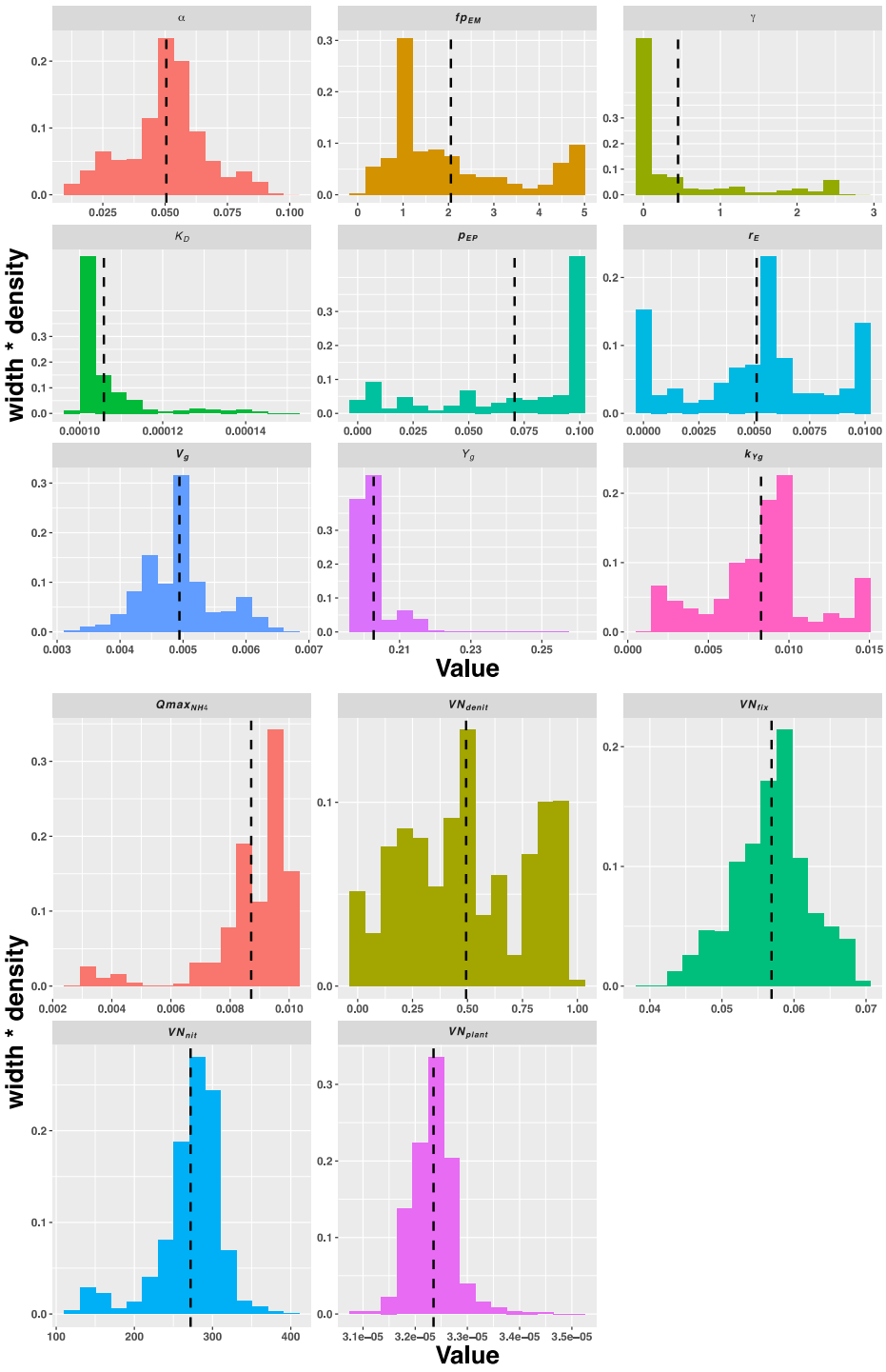

Figure S6. Posteriori distribution of parameters derived from the Uncertainty Quantification by the Critical Objective Function Index (UQ-COFI) method. See parameter description in Supplementary Table S5. "width*density" means the product of bin width and density. Vertical dashed lines denote the mean values.

5.3. MEND calibration and validation of inorganic N flux rates

Our model-data fusion results indicated that eCO_2 increased the biological N fixation rates (averagely +12% and +7% for aN and eN, respectively, see Fig. 4a) and N_2O efflux rates (+19% and +7% for aN and eN, respectively), as well as the NH_4^+ to NO_3^- ratio (+39% under aN and +9% under eN, Fig. 3c & 3d), which corroborated the previous meta-analysis [72]. However, the positive eCO_2 effects on the biological N fixation rates (Fig. 4a) or N_2O efflux rates were much lower under eN than those under aN, which meant elevated N supply could potentially alleviate N limitation in this study. Contrary to the results of Liang et al. [72], our modeling results did not show significant decreases in NO_3^- leaching in response to eCO_2 under either aN or eN, despite that there was a slight increase (+7%, p-value > 0.05) under aN and no change (+0.1%, p-value > 0.05) under eN. The insignificant main effects of eCO_2 on NO_3^- leaching had been experimentally observed at the same study site [73]. However, our modeling did not represent the impacts of plant species richness (1 or 16 species) on NO_3^- leaching as reported by Dijkstra et al. [73], suggesting that there could be large uncertainty in the estimates of NO_3^- leaching due to complicated effects of water fluxes, eCO_2, eN, and plant species.

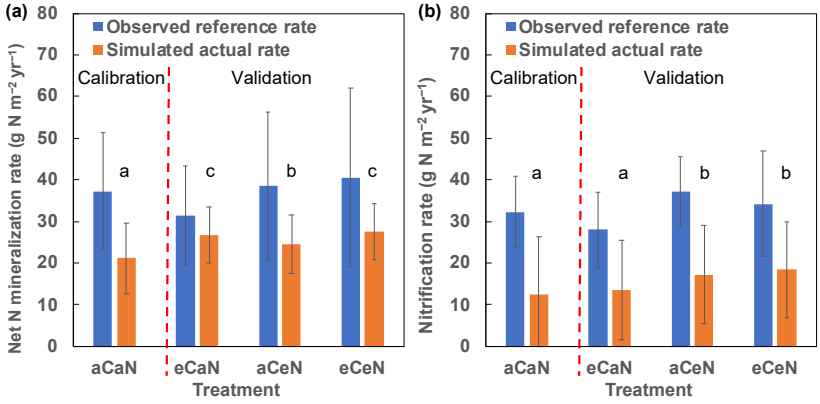

Figure S7. Comparison between simulated actual rate and observed reference rate. (a) Net N mineralization rate; **(b)** Nitrification rate. Error bars are standard deviations (n = 10). Different letters (a, b and c) above the simulated rates denote significant difference (p-value < 0.05) by the Wilcoxon signed rank test.

5.4. Elevated CO_2 effect on microbial C:N ratios

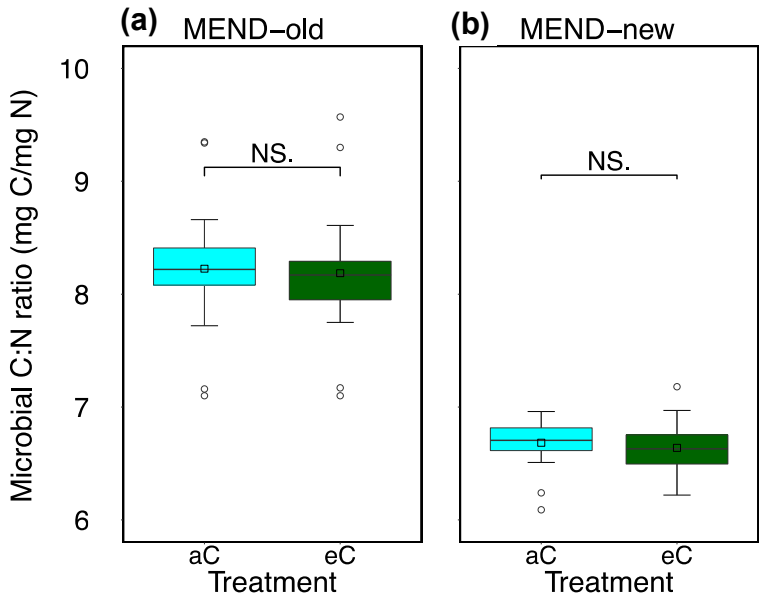

Figure S8. Comparison of elevated CO_2 effect on microbial C:N ratios simulated by two models (MEND-old and MEND-new). (a) MEND-old modeled microbial C:N ratios under ambient CO_2 concentration (aC) and elevated CO_2 concentration (eC); **(b)** MEND-new modeled microbial C:N ratios under aC and eC. MEND-old and MEND-new denote the old version of MEND model as described in Gao et al. (2020) and the new MEND model in this study, respectively. The difference between paired data was tested by the Wilcoxon signed rank test. "*", "**", and "***" denote significant difference with *p-value* < 0.05, *p-value* < 0.01, and *p-value* < 0.001, respectively. "NS." means not significant.

References

1. Gao Q, Wang G, Xue K, Yang Y, Xie J, Yu H *et al*. Stimulation of soil respiration by elevated CO_2 is enhanced under nitrogen limitation in a decade-long grassland study. Proc Natl Acad Sci USA 2020; 117: 33317-33324.
2. Wang G, Huang W, Zhou G, Mayes MA, Zhou J. Modeling the processes of soil moisture in regulating microbial and carbon-nitrogen cycling. J Hydrol 2020; 585: 124777.
3. Wang G, Jagadamma S, Mayes MA, Schadt CW, Steinweg JM, Gu L *et al*. Microbial dormancy improves development and experimental validation of ecosystem model. ISME J 2015; 9: 226-237.
4. Wang G, Huang W, Mayes MA, Liu X, Zhang D, Zhang Q *et al*. Soil moisture drives microbial controls on carbon decomposition in two subtropical forests. Soil Biol Biochem 2019; 130: 185-194.
5. Wang G, Post WM, Mayes MA. Development of microbial-enzyme-mediated decomposition model parameters through steady-state and dynamic analyses. Ecol Appl 2013; 23: 255-272.
6. Zhou J, Xue K, Xie J, Deng Y, Wu L, Cheng X *et al*. Microbial mediation of carbon-cycle feedbacks to climate warming. Nat Clim Change 2012; 2: 106-110.
7. Xue K, Yuan MM, Shi ZJ, Qin Y, Deng Y, Cheng L *et al*. Tundra soil carbon is vulnerable to rapid microbial decomposition under climate warming. Nat Clim Change 2016; 6: 595-600.
8. Thornton PE, Rosenbloom NA. Ecosystem model spin-up: Estimating steady state conditions in a coupled terrestrial carbon and nitrogen cycle model. Ecol Modell 2005; 189: 25-48.
9. Bonan GB, Hartman MD, Parton WJ, Wieder WR. Evaluating litter decomposition in earth system models with long-term litterbag experiments: an example using the Community Land Model version 4 (CLM4). Global Change Biol 2013; 19: 957-974.
10. Fanin N, Fromin N, Barantal S, Hättenschwiler S. Stoichiometric plasticity of microbial communities is similar between litter and soil in a tropical rainforest. Sci Rep 2017; 7: 12498.
11. Du Z, Weng E, Jiang L, Luo Y, Xia J, Zhou X. Carbon–nitrogen coupling under three schemes of model representation: a traceability analysis. Geosci Model Dev 2018; 11: 4399-4416.

12. Mooshammer M, Wanek W, Zechmeister-Boltenstern S, Richter AA. Stoichiometric imbalances between terrestrial decomposer communities and their resources: mechanisms and implications of microbial adaptations to their resources. Front Microbiol 2014; 5: Article 22.

13. Mooshammer M, Wanek W, Hämmerle I, Fuchslueger L, Hofhansl F, Knoltsch A *et al*. Adjustment of microbial nitrogen use efficiency to carbon: nitrogen imbalances regulates soil nitrogen cycling. Nat Commun 2014; 5: 3694.

14. Zechmeister-Boltenstern S, Keiblinger KM, Mooshammer M, Peñuelas J, Richter A, Sardans J *et al*. The application of ecological stoichiometry to plant–microbial–soil organic matter transformations. Ecol Monogr 2015; 85: 133-155.

15. Schimel JP, Weintraub MN. The implications of exoenzyme activity on microbial carbon and nitrogen limitation in soil: a theoretical model. Soil Biol Biochem 2003; 35: 549-563.

16. Cleveland CC, Liptzin D. C : N : P stoichiometry in soil: is there a "Redfield ratio" for the microbial biomass? Biogeochemistry 2007; 85: 235-252.

17. Johnson KA, Goody RS. The Original Michaelis Constant: Translation of the 1913 Michaelis–Menten Paper. Biochemistry 2011; 50: 8264-8269.

18. Wang G, Post WM. A note on the reverse Michaelis–Menten kinetics. Soil Biol Biochem 2013; 57: 946-949.

19. Wang G, Post WM. A theoretical reassessment of microbial maintenance and implications for microbial ecology modeling. FEMS Microbiol Ecol 2012; 81: 610-617.

20. Wang G, Mayes MA, Gu L, Schadt CW. Representation of dormant and active microbial dynamics for ecosystem modeling. PLoS One 2014; 9: e89252.

21. Stolpovsky K, Martinez-Lavanchy P, Heipieper HJ, Van Cappellen P, Thullner M. Incorporating dormancy in dynamic microbial community models. Ecol Modell 2011; 222: 3092-3102.

22. Jian S, Li J, Chen J, Wang G, Mayes MA, Dzantor KE *et al*. Soil extracellular enzyme activities, soil carbon and nitrogen storage under nitrogen fertilization: A meta-analysis. Soil Biol Biochem 2016; 101: 32-43.

23. Sinsabaugh RL, Belnap J, Findlay SG, Shah JJF, Hill BH, Kuehn KA *et al*. Extracellular enzyme kinetics scale with resource availability. Biogeochemistry 2014; 121: 287-304.

24. Fiencke C, Bock E. Immunocytochemical localization of membrane-bound ammonia monooxygenase in cells of ammonia oxidizing bacteria. Arch Microbiol 2006; 185: 99-106.

25. Schlesier J, Rohde M, Gerhardt S, Einsle O. A conformational switch triggers nitrogenase protection from oxygen damage by Shethna protein II (FeSII). J Am Chem Soc 2016; 138: 239-247.

26. Song H-S, Thomas DG, Stegen JC, Li M, Liu C, Song X *et al*. Regulation-structured dynamic metabolic model provides a potential mechanism for delayed enzyme response in denitrification process. Front Microbiol 2017; 8: 1866.

27. Sinsabaugh RL, Manzoni S, Moorhead DL, Richter A. Carbon use efficiency of microbial communities: stoichiometry, methodology and modelling. Ecol Lett 2013; 16: 930-939.

28. Spohn M. Microbial respiration per unit microbial biomass depends on litter layer carbon-to-nitrogen ratio. Biogeosciences 2015; 12: 817-823.

29. Tang JY, Riley WJ. A total quasi-steady-state formulation of substrate uptake kinetics in complex networks and an example application to microbial litter decomposition. Biogeosciences 2013; 10: 8329-8351.

30. Carvalho TLG, Balsemão-Pires E, Saraiva RM, Ferreira PCG, Hemerly AS. Nitrogen signalling in plant interactions with associative and endophytic diazotrophic bacteria. Journal of Experimental Botany 2014; 65: 5631-5642.

31. Zhu X, Burger M, Doane TA, Horwath WR. Ammonia oxidation pathways and nitrifier denitrification are significant sources of N2O and NO under low oxygen availability. Proc Natl Acad Sci USA 2013; 110: 6328-6333.

32. Wrage-Mönnig N, Horn MA, Well R, Müller C, Velthof G, Oenema O. The role of nitrifier denitrification in the production of nitrous oxide revisited. Soil Biol Biochem 2018; 123: A3-A16.

33. Fernando W, Xia K, Rice CW. Sorption and desorption of ammonium from liquid swine waste in soils. Soil Sci Soc Am J 2005; 69: 1057-1065.

34. Neitsch SL, Arnold JG, Kiniry JR, Williams JR: **Soil and Water Assessment Tool Theoretical Documentation. Version 2009**. In. College Station, TX: Texas Water Resources Institute, Texas A&M University System; 2011: 647.

35. Jones SB, Or D, Bingham GE. Gas diffusion measurement and modeling in coarse-textured porous media. Vadose Zone Journal 2003; 2: 602-610.

36. Potter CS, Davidson EA, Verchot LV. Estimation of global biogeochemical controls and seasonality in soil methane consumption. Chemosphere 1996; 32: 2219-2246.

37. Wang G, Chen S. Evaluation of a soil greenhouse gas emission model based on Bayesian inference and MCMC: Model uncertainty. Ecol Modell 2013; 253: 97-106.

38. Wang G, Post WM, Mayes MA, Frerichs JT, Jagadamma S. Parameter estimation for models of ligninolytic and cellulolytic enzyme kinetics. Soil Biol Biochem 2012; 48: 28-38.

39. Devevre OC, Horwath WR. Decomposition of rice straw and microbial carbon use efficiency under different soil temperatures and moistures. Soil Biol Biochem 2000; 32: 1773-1785.

40. Tucker CL, Bell J, Pendall E, Ogle K. Does declining carbon-use efficiency explain thermal acclimation of soil respiration with warming? Global Change Biol 2013; 19: 252-263.

41. Frey SD, Lee J, Melillo JM, Six J. The temperature response of soil microbial efficiency and its feedback to climate. Nat Clim Change 2013; 3: 395-398.

42. Steinweg JM, Plante AF, Conant RT, Paul EA, Tanaka DL. Patterns of substrate utilization during long-term incubations at different temperatures. Soil Biol Biochem 2008; 40: 2722-2728.

43. Fieschko J, Humphrey AE. Statistical analysis in the estimation of maintenance and true growth yield coefficients. Biotechnol Bioeng 1984; 26: 394-396.

44. Steinweg JM, Dukes JS, Wallenstein MD. Modeling the effects of temperature and moisture on soil enzyme activity: Linking laboratory assays to continuous field data. Soil Biol Biochem 2012; 55: 85-92.

45. Hansen S, Jensen HE, Nielsen NE, Svendsen H: **DAISY-Soil plant atmosphere system model**. In. Copenhagen, Denmark: The Royal Veterinary and Agricultural University; 1990: 272.

46. Manzoni S, Schimel JP, Porporato A. Responses of soil microbial communities to water stress: results from a meta-analysis. Ecology 2012; 93: 930-938.

47. Manzoni S, Schaeffer SM, Katul G, Porporato A, Schimel JP. A theoretical analysis of microbial eco-physiological and diffusion limitations to carbon cycling in drying soils. Soil Biol Biochem 2014; 73: 69-83.

48. Muller C: **Modeling soil-biosphere interactions**. New York, NY: CABI Publishing; 1999.

49. Xu X, Thornton PE, Post WM. A global analysis of soil microbial biomass carbon, nitrogen and phosphorus in terrestrial ecosystems. Global Ecology and Biogeography 2013; 22: 737-749.

50. Sulman BN, Moore JA, Abramoff R, Averill C, Kivlin S, Georgiou K *et al*. Multiple models and experiments underscore large uncertainty in soil carbon dynamics. Biogeochemistry 2018; 141: 109-123.

51. van Genuchten MT. A closed-form equation for predicting the hydraulic conductivity of unsaturated soils. Soil Sci Soc Am J 1980; 44: 892-898.

52. Tuller M, Or D. Retention of water in soil and the soil water characteristic curve. Encyclopedia of Soils in the Environment 2004; 4: 278-289.

53. Liang J, Wang G, Ricciuto DM, Gu L, Hanson PJ, Wood JD *et al*. Evaluating the E3SM Land Model version 0 (ELMv0) at a temperate forest site using flux and soil water measurements. Geoscientific Model Development 2019; 12: 1601-1612.

54. Mueller KE, Hobbie SE, Tilman D, Reich PB. Effects of plant diversity, N fertilization, and elevated carbon dioxide on grassland soil N cycling in a long‐term experiment. Global Change Biol 2013; 19: 1249-1261.

55. Refsgaard JC. Parameterisation, calibration and validation of distributed hydrological models. J Hydrol 1997; 198: 69-97.

56. Wang G, Chen S. A review on parameterization and uncertainty in modeling greenhouse gas emissions from soil. Geoderma 2012; 170: 206-216.

57. Conover WJ: **Practical Nonparametric Statistics, 3rd Edition**. New York: John Wiley & Sons; 1998.

58. Zhang XY, Trame M, Lesko L, Schmidt S. Sobol sensitivity analysis: a tool to guide the development and evaluation of systems pharmacology models. CPT: pharmacometrics & systems pharmacology 2015; 4: 69-79.

59. Duan QY, Sorooshian S, Gupta V. Effective and efficient global optimization for conceptual rainfall-runoff models. Water Resour Res 1992; 28: 1015-1031.

60. Wang G, Jager HI, Baskaran LM, Brandt CC. Hydrologic and water quality responses to biomass production in the Tennessee River Basin. Global Change Biol Bioenergy 2018; 10: 877-893.

61. Cleveland CC, Townsend AR, Schimel DS, Fisher H, Howarth RW, Hedin LO *et al*. Global patterns of terrestrial biological nitrogen (N_2) fixation in natural ecosystems. Global Biogeochem Cycles 1999; 13: 623-645.

62. Fisher JB, Sitch S, Malhi Y, Fisher RA, Huntingford C, Tan SY. Carbon cost of plant nitrogen acquisition: A mechanistic, globally applicable model of plant nitrogen uptake, retranslocation, and fixation. Global Biogeochem Cycles 2010; 24: GB1014.

63. Reyes J, Schellberg J, Siebert S, Elsaesser M, Adam J, Ewert F. Improved estimation of nitrogen uptake in grasslands using the nitrogen dilution curve. Agron Sustain Dev 2015; 35: 1561-1570.

64. Wang G, Li W, Wang K, Huang W. Uncertainty quantification of the soil moisture response functions for microbial dormancy and resuscitation. Soil Biol Biochem 2021; 160: 108337.

65. Wang G, Xia J, Chen J. Quantification of effects of climate variations and human activities on runoff by a monthly water balance model: A case study of the Chaobai River basin in northern China. Water Resour Res 2009; 45: W00A11.

66. Wang G, Xia J. Improvement of SWAT2000 modelling to assess the impact of dams and sluices on streamflow in the Huai River basin of China. Hydrological Processes 2010; 24: 1455-1471.

67. Zhang X, Srinivasan R, Zhao K, Liew MV. Evaluation of global optimization algorithms for parameter calibration of a computationally intensive hydrologic model. Hydrological Processes 2009; 23: 430-441.

68. Duan QY, Sorooshian S, Gupta VK. Optimal use of the SCE-UA global optimization method for calibrating watershed models. J Hydrol 1994; 158: 265-284.

69. Batstone DJ, Pind PF, Angelidaki I. Kinetics of thermophilic, anaerobic oxidation of straight and branched chain butyrate and valerate. Biotechnol Bioeng 2003; 84: 195-204.

70. Gross J, Ligges U. R Package 'nortest': Tests for Normality (version 01.0-4). 2015. https://cran.r-project.org/web/packages/nortest/index.html.

71. Refsgaard JC, van der Sluijs JP, Hojberg AL, Vanrolleghem PA. Uncertainty in the environmental modelling process - A framework and guidance. Environ Modell Softw 2007; 22: 1543-1556.

72. Liang J, Qi X, Souza L, Luo Y. Processes regulating progressive nitrogen limitation under elevated carbon dioxide: a meta-analysis. Biogeosciences 2016; 13: 2689-2699.

73. Dijkstra FA, West JB, Hobbie SE, Reich PB, Trost J. Plant diversity, CO_2, and N influence inorganic and organic N leaching in grasslands. Ecology 2007; 88: 490-500.